# Simultaneously Dual Modification of Li-Rich and Mn-Based Cathode in Restraining Oxygen Release and Structure Distortion

Shaowei Kang ‡,[1, 2] Xianbin Wei ‡,[3] Youqi Chu ‡, [1, 2] Yongbiao Mu, [1, 2] Lingfeng Zou, [1, 2] Xiaoqian Xu, [1, 2] Qing Zhang*,[1, 2] Lin Zeng*,[1, 2]

[1]Shenzhen Key Laboratory of Advanced Energy Storage, Department of Mechanical and Energy Engineering, Southern University of Science and Technology, Shenzhen 518055, China

[2]SUSTech Energy Institute for Carbon Neutrality, Southern University of Science and Technology, Shenzhen 518055, China

[3]Department of Materials Science and Engineering, Southern University of Science and Technology, Shenzhen 518055, China

‡ These authors contributed equally.

* Corresponding authors.

E-mail addresses: zhangq6@sustech.edu.cn (Q. Zhang); zengl3@sustech.edu.cn (L. Zeng)

Tel/Fax:0000-0003-2426-7095; Tel/Fax:0000-0002-0510-1754

**Experimental section**

***1.1 Synthesis of LRM and CB-LRM:*** Carbonate precursor of $Ni_{0.167}Co_{0.167}Mn_{.666}CO_3$ were prepared by co-precipitation. First, a certain number of sulfates were dispersed by deionized water (2 M, Ni: Co: Mn molar ratio=1:1:4). $Na_2CO_3$ solution (2 M) and appropriate $NH_4OH$ were continuously in folded above solution. The reaction kettle temperature was controlled at 50 °C and the pH was controlled at 11.0. Finally, the compounds were stirred for 16 h and aged for 24 h, the carbonate precursor was washed, collected, and dried at 80 ºC. Next, precursors with befitting $Li_2CO_3$ to prepare LRM, after calcined 480 ºC for 5 h and 880 ºC for 12 h in $O_2$. Furthermore, the cathode was added dropwise into the solution of contain cerium stirring for 0.5 h, denoted as A. Subsequently, 10 ml boric acid ethanol solution was slowly added into A and kept 2 h under stirring and Ar atmosphere. In the second step, CB-LRM was calcined for 2h at Ar, Ce, B-LRM@$CeO_2$ (denoted as CBLRM).

***1.2 Materials Characterizations:*** Morphologies of the active materials and the battery electrodes were observed by using field emission scanning electron microscopy (FESEM, JEOL JSM-7600F, 5 kV) and transmission electron microscopy (TEM, Talos F200X G2). Data for X-ray diffraction were acquired using a Bruker D8 Advance X-ray diffractometer outfitted with a *LynxEye* 1-dimensional detector with Cu-Ka radiation at 40 kV and 40 mA ($\lambda$ = 1.5418 Å) with a step increment of 0.02 and a duration per step of 0.8 s. Rietveld refinement of the powder diffraction patterns was analyzed by the software (GSAS program) based on the crystal model of $Li_{1.184}Ni_{0.136}Co_{0.136}Mn_{0.544}O_2$ with a space group of *R-3m* and *C/2m*. X-ray photoelectron spectroscopy (XPS) measurements were performed on Thermo Kalpha with an automated dual-anode X-ray monochromatic source.

***1.3 Fabrication of electrodes:*** The mixtures were cast on Al foil, in which active materials (85 wt%), binder (PVDF, 5 wt%), and conductive agent (Super-P, 10 wt%). The electrodes were dried at 80 ºC for 12 h.

***1.4 Electrochemical measurements:*** The 2025R coin-type cells were assembled in an argon-filled glove box (the moisture and oxygen concentrations are ≤0.01 ppm) with

lithium foil as the reference electrode, and the electrolyte of 1 M $LiPF_6$ in ethylene carbonate/diethyl carbonate/dimethyl carbonate (EC: DEC: EMC=1:1:1 in volume). The charge/discharge of half cells was carried out at multifarious current densities and the voltage range of ≈2.0-4.8 V on a LAND battery tester.

*1.5 Determination of lithium diffusion coefficient by galvanostatic intermittent titration technique (GITT):* The cell was first charged from open circuit voltage at a $\tau$ = 15 min under a current pulse of 0.2 C, followed by a relaxation time of 30 min to allow the system to reach electrochemical equilibrium, and the operation is repeated, until the end of the voltage window. The GITT curves of the NCM811/Li half-cell in the 10th cycle. The D Li + was calculated by the following **Eq. (1):**

$$D_{Li^+} = \frac{4}{\pi \tau}\left(\frac{m_B V_M}{M_B S}\right)^2 \left(\frac{\Delta E_s}{\Delta E_\tau}\right)^2 \ (\tau \ll L^2/D_{Li^+})$$

where $m_B$ is the mass loading (g), $V_M$ is the molar volume ($cm^3 \ mol^{-1}$), $M_B$ is the molecular weight ($g \ mol^{-1}$), A is the contact area of the electrode ($cm^2$), and $\tau$ is the time when the current pulse is applied (s), $\Delta E_s$ is the voltage difference between the steady-state potentials before and after the current pulse, and $\Delta E_\tau$ is the voltage difference between the cell potential at the start and the end of the current pulse.


*1.6 Calculation method:*

The density functional theory (DFT) calculations[1, 2] were carried out in the Vienna *ab initio* simulation package (VASP) based on the plane-wave basis sets with the projector augmented-wave method.[3, 4] The exchange-correlation potential was treated by using a generalized gradient approximation (GGA) with the Perdew-Burke-Ernzerhof (PBE) parametrization.[5] The energy cutoff was set to be 520 eV. The Brillouin-zone integration was sampled with a Γ-centered Monkhorst-Pack mesh of 2× 2 × 1.[6] The structures were fully relaxed until the maximum force on each atom was less than 0.01 eV per Å, and the energy convergent standard was $10^{-5}$ eV. A Gaussian smearing with a width of 0.05 eV for the occupation of the electronic level was used. The van der Waals correction of Grimme's DFT-D3 model was also adopted.[7] Following previous works,[8] the effective Hubbard approach is used for Co/Mn/Ni elements. The formation

energy was computed from:

$$E_f=(E_{bulk}-x\mu_i)/n$$

where $E_{bulk}$ is the total energy of the simulated bulk structure, $x\mu i$ means the total energy of the number of $x_i$ atoms in the corresponding bulk phase, and represents the total number of atoms in the system, respectively.

The oxygen vacancy formation energy $\Delta_{Eform}$ was computed from:

$$\Delta_{Eform}=E_{tot,Vo}-E_{tot}+\mu O$$

Here $\mu O$ are the strain and the oxygen chemical potential. $E_{tot}$ and $E_{tot,Vo}$ denote the DFT total energy of the simulation cell and that containing one oxygen vacancy respectively.
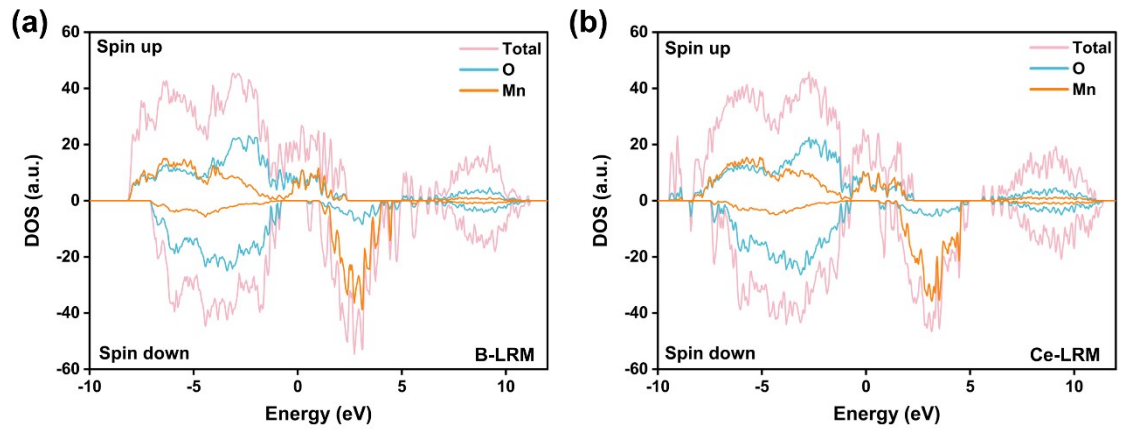
**Figure S1.** The calculated Density of State of (a) B-LRM and (b) Ce-LRM.
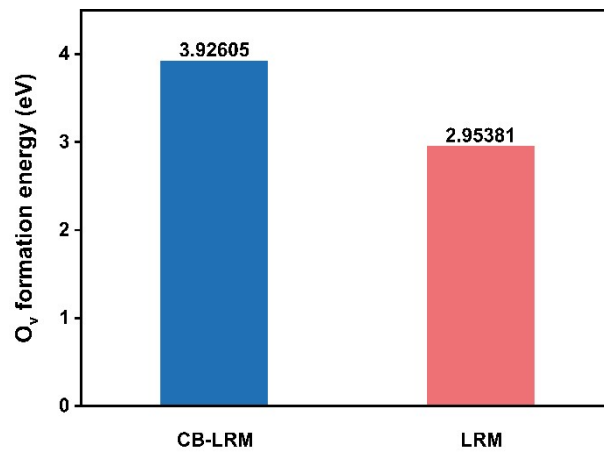


**Figure S2.** The formation energy of oxygen vacancies for CB-LRM and LRM.
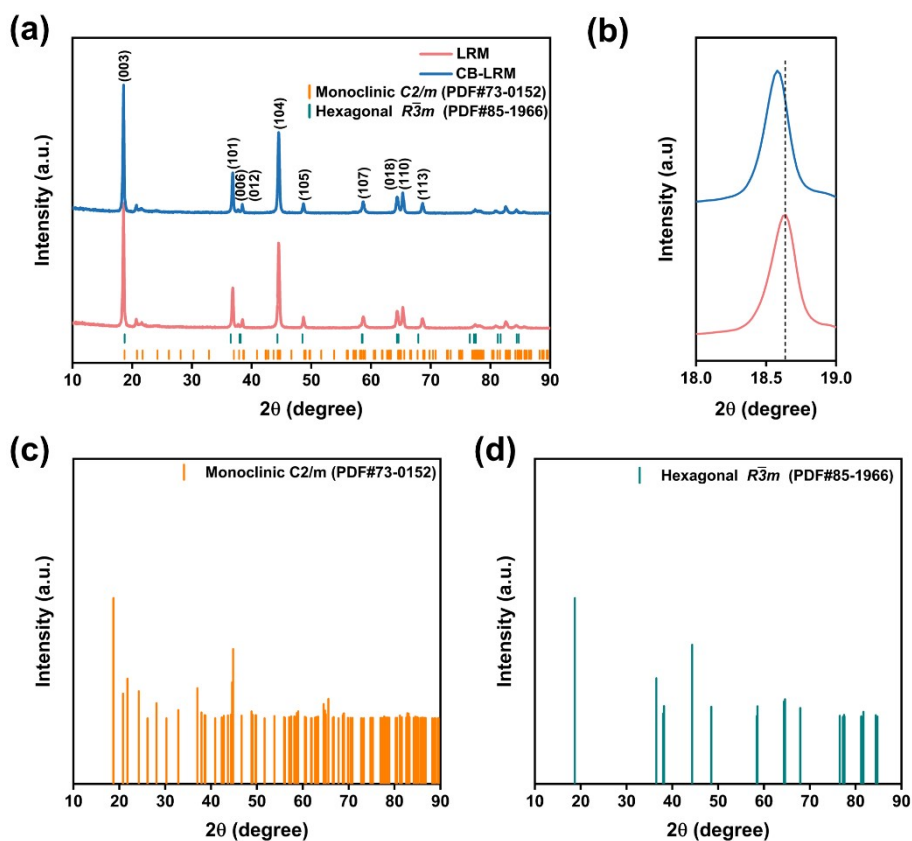
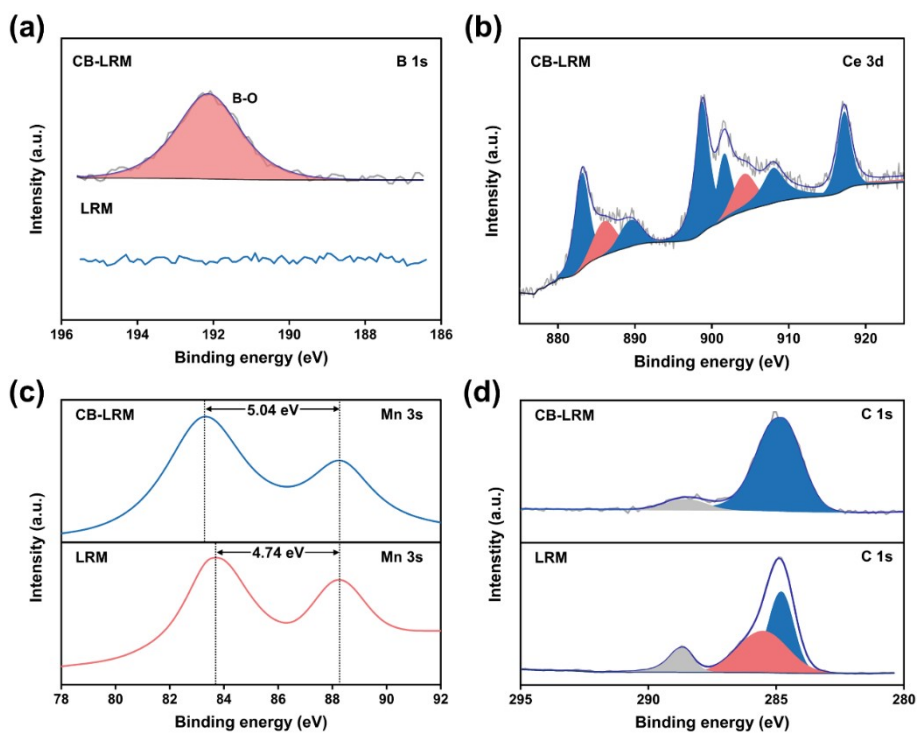**Figure S3.** The X-ray powder diffraction patterns and corresponding PDF of LRM and CB-LRM.



**Figure S4.** XPS spectra of LRM and CB-LRM samples: (a) C *1s*, (b) Mn *3s*, (c) Ce *3d*, and (d) B
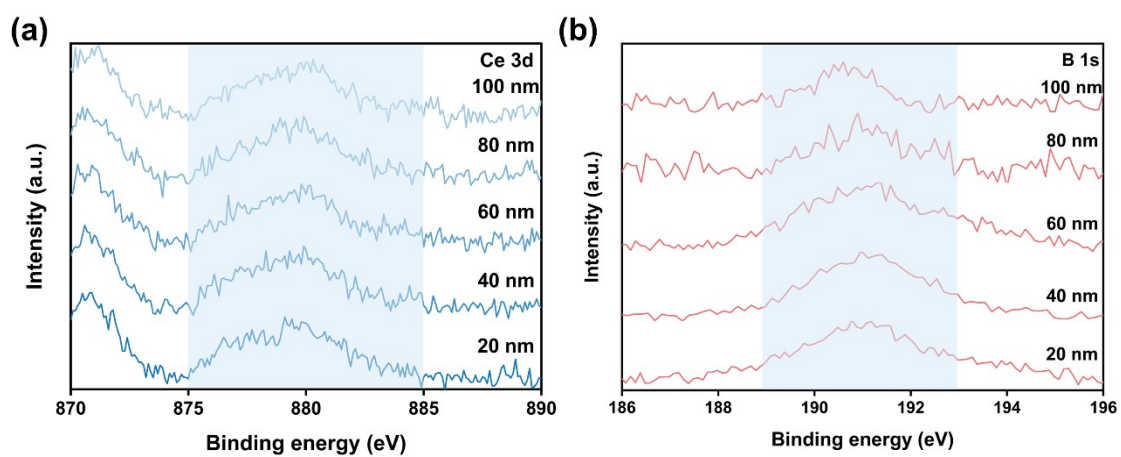
*1s*.

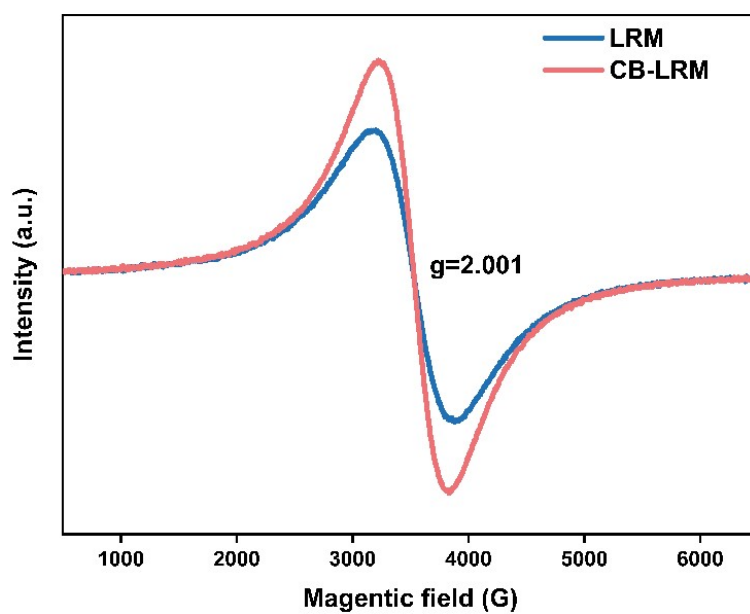**Figure S5.** The XPS spectra of B 1s and Ce 3d for CB-LRM at different etching depths.
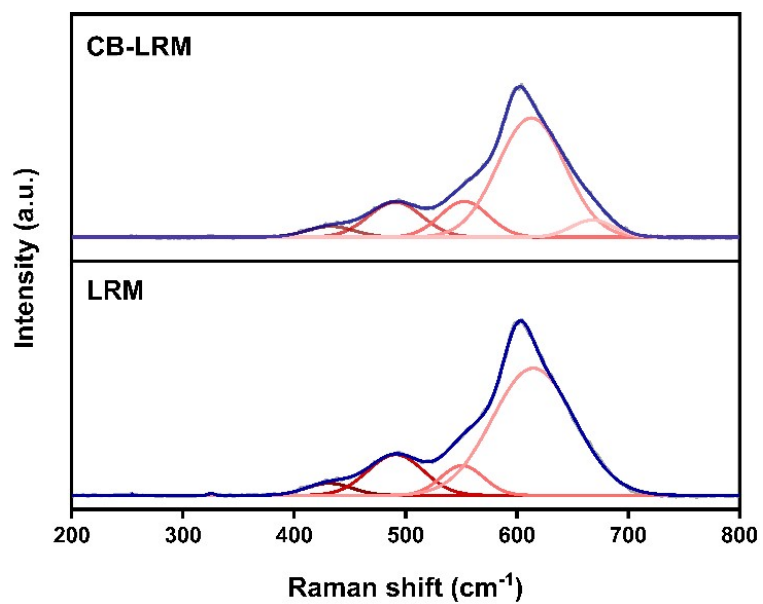


**Figure S6.** EPR spectra of LRM and CB-LRM samples.

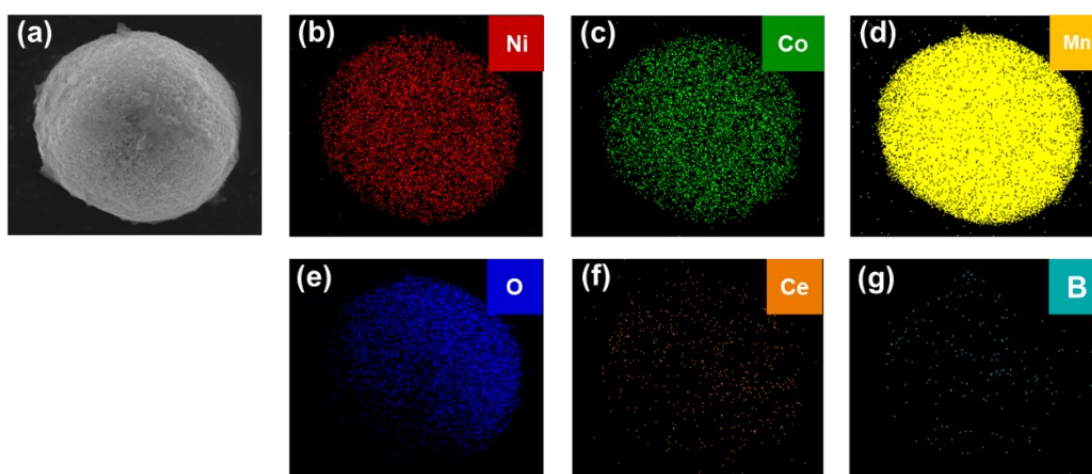**Figure S7.** Raman spectra of LRM and CB-LRM samples.



**Figure S8.** (a-g) SEM-EDS images showing the elements uniformly distributed in CB-LRM.
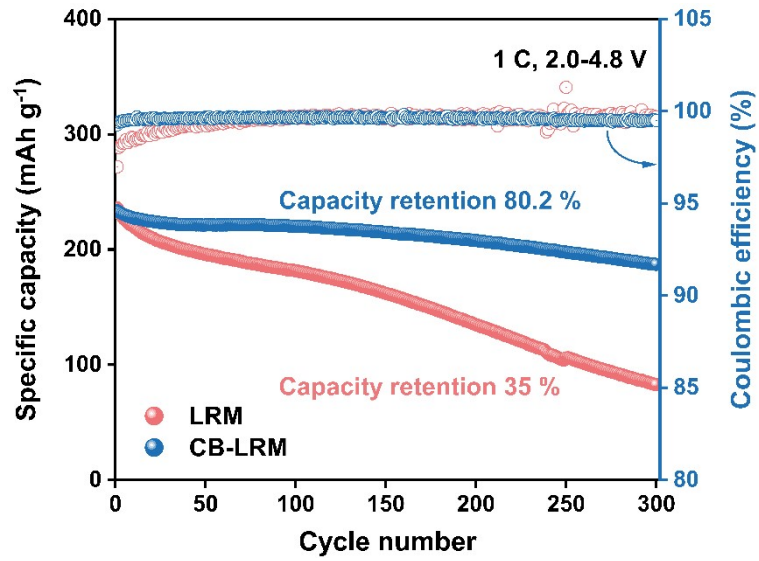
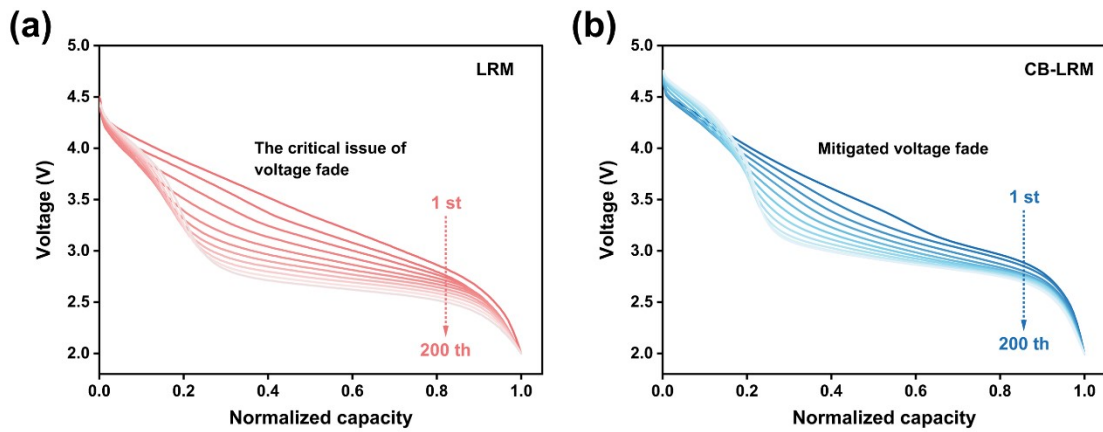**Figure S9.** The cycle performance of LRM and CB-LRM after 300 cycles.



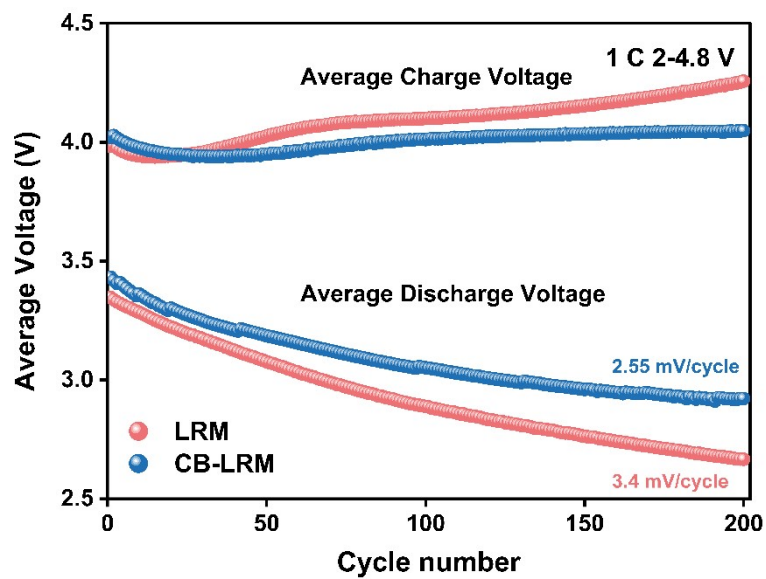**Figure S10.** The voltage-capacity curves of (a) LRM and (b) CB-LRM.

**Figure S11.** The average voltage attenuation rate of CB-LRM and LRM.
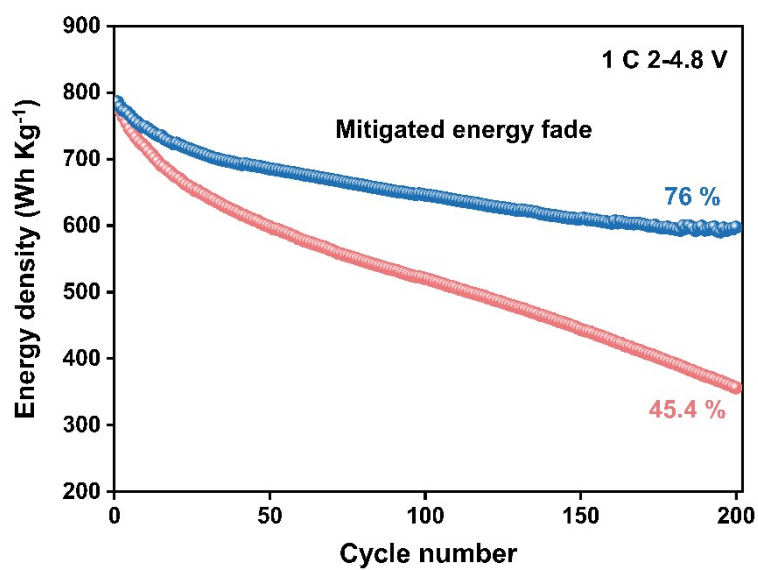


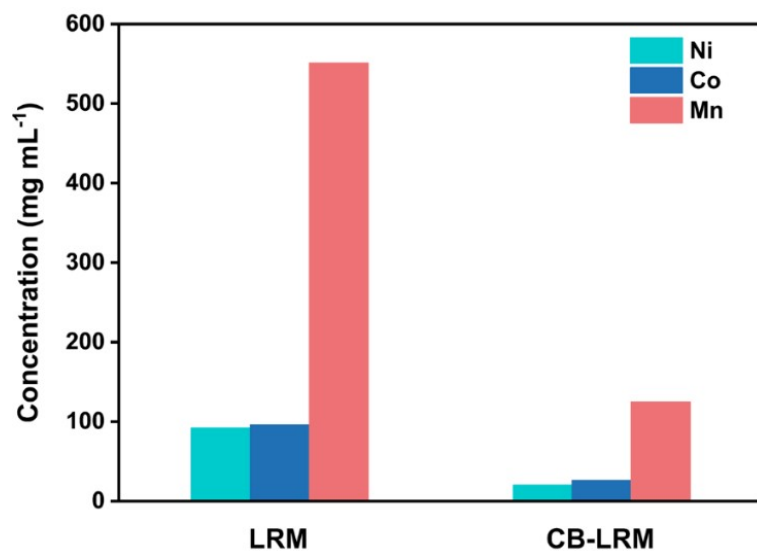**Figure S12.** The energy density curves of LRM and CB-LRM.

**Figure S13.** ICP-AES analysis data for Transition metal content of LRM and CB-LRM electrodes after 200 cycles.
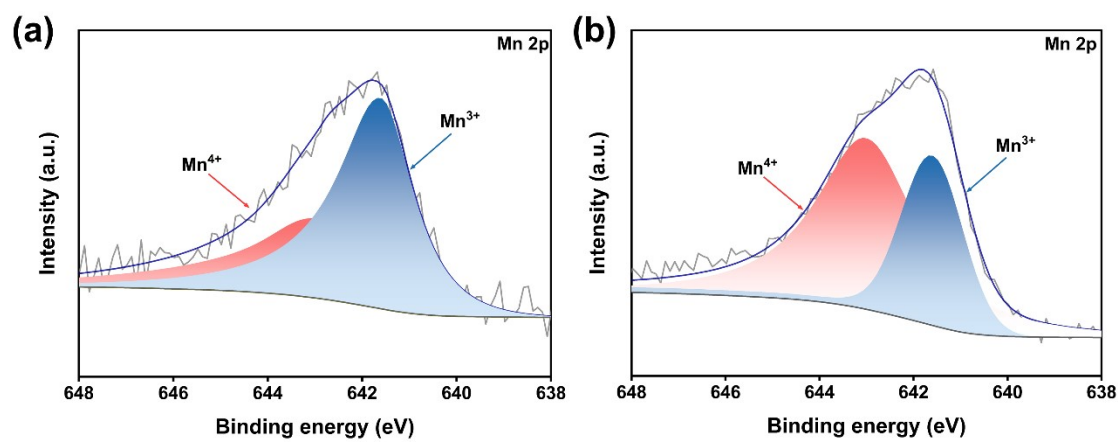


**Figure S14.** The XPS spectrum of Mn 2p for LRM and CB-LRM sample after 200 cycles.

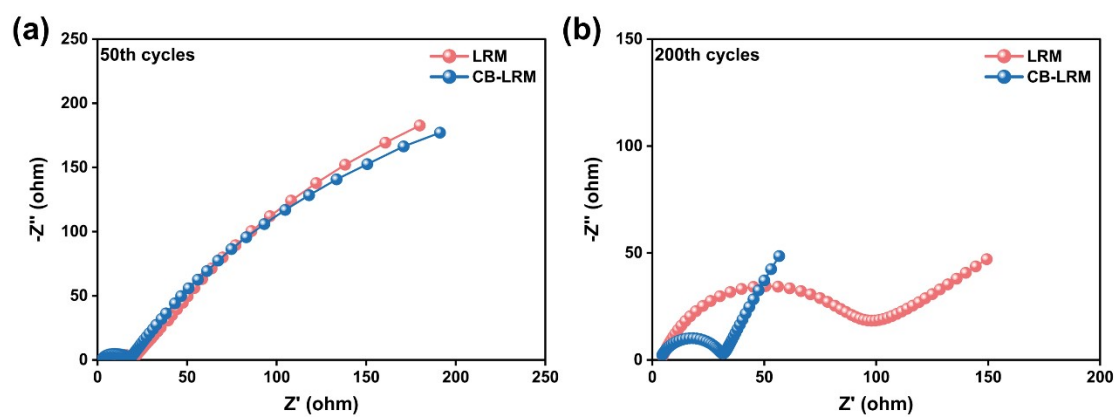**Figure S15.** EIS plots of LRM and CB-LRM in the charged state of 4.8 V 50th and 200th cycles.
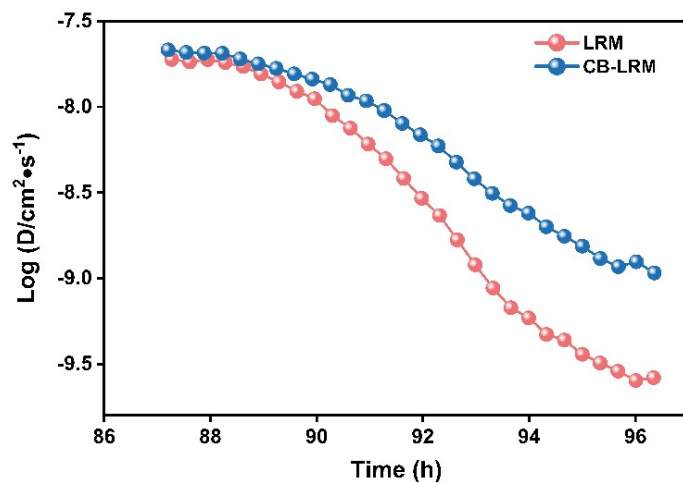


**Figure S16.** GITT calculated the Li$^+$ diffusion coefficient in LRM and CB-LRM during
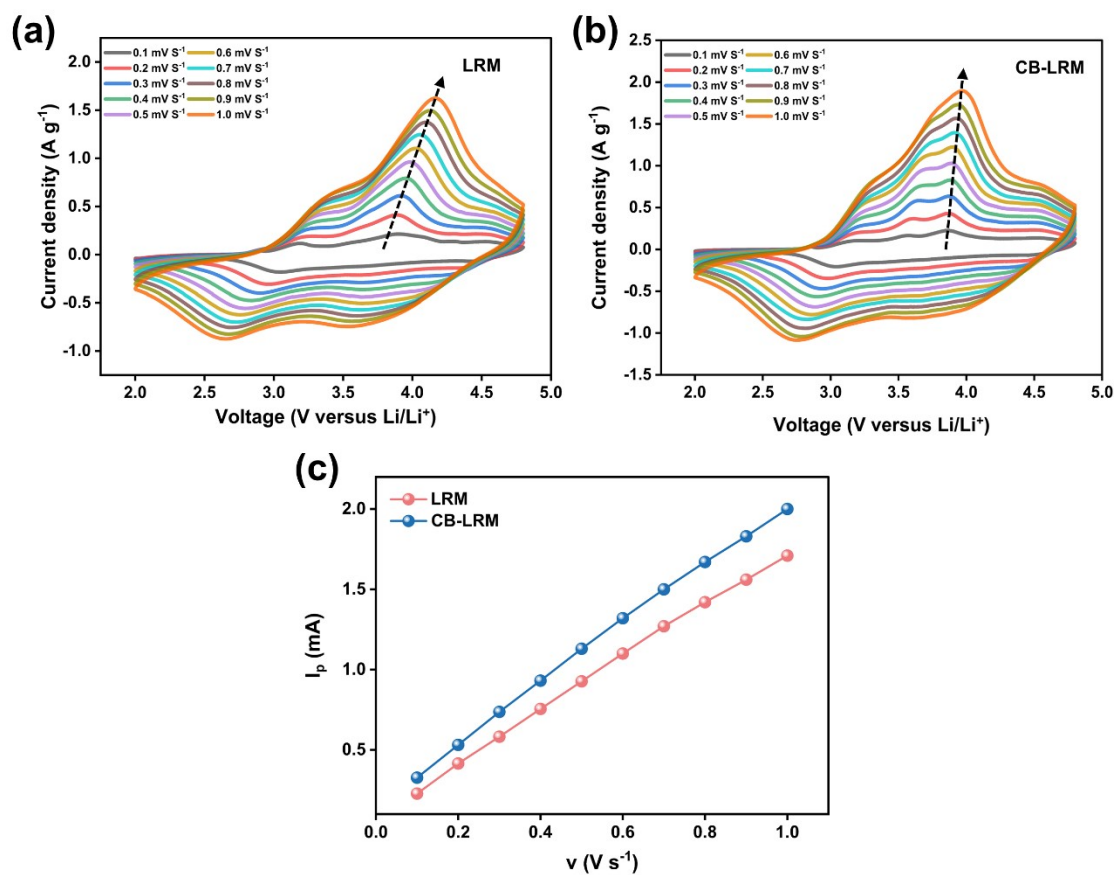
discharging processes.

**Figure S17.** The CV curves of (a) LRM and (b) CB-LRM electrodes at varied sweep rates from 0.1 to 1 mVs⁻¹, and (c) the corresponding plotted relationship between peak current density and sweep.

**Table S1.** ICP analysis data for the atomic compositions of LRM and CB-LRM.

| Samples | Mole ratio over (Ni+Co+Mn) (%) | | | |
|---|---|---|---|---|
| | Li | Ni | Co | Mn |
| **LRM** | 1.189 | 0.134 | 0.129 | 0.535 |
| **CB-LRM** | 1.193 | 0.138 | 0.127 | 0.541 |

**Table S2.** XRD Rietveld refinement results of lattice parameters for LRM and CB-LRM.

| | a(Å) | b(Å) | c(Å) | Cation mix (%) | LiMO$_2$ (wt %) | Li$_2$MnO$_3$ (wt %) |
|---|---|---|---|---|---|---|
| **LRM** | Space group: *R-3m* | | | 4.2 | 80.5 | 19.5 |
| | 2.85113 | 2.85113 | 14.24057 | | | |
| | Space group: *C/2m* | | | | | |
| | 4.94502 | 8.53016 | 5.04707 | | | |
| **CB-LRM** | Space group: *R-3m* | | | 3.3 | 85.44 | 14.56 |
| | 2.85074 | 2.85074 | 14.24068 | | | |
| | Space group: *C2/m* | | | | | |
| | 4.94384 | 8.52956 | 5.05047 | | | |

**Table S3.** Capacity retention of CB-LRM with other previously reported Li-rich Mn-based cathode materials.

| Samples | Current density | Cycles | Capacity retention | Reference |
|---|---|---|---|---|
| Gas-treated $Li_{1.2}Ni_{0.2}Mn_{0.6}O_2$ | 1 C | 200 | 77.2 % | [9] |
| $AlF_3$-coating $Li_{1.2}Ni_{0.2}Mn_{0.6}O_2$ | 300 mAh $g^{-1}$ | 100 | 88 % | [10] |
| Al, Nd-doping $Li_{1.2}Mn_{0.533}Ni_{0.267}O_2$ | 1 C | 100 | 90 % | [11] |
| $Li_2SiO_3$-coated $Li_{1.13}Ni_{0.3}Mn_{0.57}O_2$ | 1 C | 200 | 86.6 % | [12] |
| $CeO_2$-$Li_{1.2}Mn_{0.53}Ni_{0.27}O_2$ | 1 C | 200 | 80.2 % | [13] |
| $Li_{1.2}Mn_{0.585}Ni_{0.185}Fe_{0.03}O_2$ | 1 C | 200 | 80 % | [14] |
| $SeO_2$ infuse $Li_{1.2}Mn_{0.54}Ni_{0.13}Co_{0.13}O_2$ | 1 C | 200 | 80 % | [15] |
| Sb-doping $Li_{1.2}Ni_{0.2}Mn_{0.6}O_2$ | 1 C | 200 | 86.3 % | [16] |
| $LiNbO_3$-coating $Li_{1.2}Mn_{0.54}Ni_{0.13}Co_{0.13}O_2$ | 1 C | 250 | 74.05 % | [17] |
| $Li_4V_2Mn(PO_4)_4$-coating $Li_{1.2}Mn_{0.54}Ni_{0.13}Co_{0.13}O_2$ | 1 C | 200 | 84.2 % | [18] |
| Ce, B co-doping and $CeO_2$ coating $Li_{1.184}Ni_{0.136}Co_{0.136}Mn_{0.544}O_2$ | 1 C | 200 | 89.6 % | This work |

# References

1.    P. Hohenberg and W. Kohn, *Physical review*, 1964, **136**, B864.

2.    W. Kohn and L. J. Sham, *Physical review*, 1965, **140**, A1133.

3.    J. J. Mortensen, L. B. Hansen and K. W. Jacobsen, *Physical review B*, 2005, **71**, 035109.

4.    S. Lebegue and O. Eriksson, *Physical Review B*, 2009, **79**, 115409.

5.    J. P. Perdew, K. Burke and M. Ernzerhof, *Phys. Rev. Lett.*, 1996, **77**, 3865.

6.    H. J. Monkhorst and J. D. Pack, *Physical review B*, 1976, **13**, 5188.

7.    W. Reckien, F. Janetzko, M. F. Peintinger and T. Bredow, *J. Comput. Chem.*, 2012, **33**, 2023-2031.

8.    A. A. Emery and C. Wolverton, *Sci. Data*, 2017, **4**, 1-10.

9.    L. Bao, L. Wei, N. Fu, J. Dong, L. Chen, Y. Su, N. Li, Y. Lu, Y. Li and S. Chen, *Journal of Energy Chemistry*, 2022, **66**, 123-132.

10.   A. Abdel-Ghany, A. M. Hashem, A. Mauger and C. M. Julien, *Energies*, 2020, **13**, 3487.

11.   W. Jiang, C. Zhang, Y. Feng, B. Wei, L. Chen, R. Zhang, D. G. Ivey, P. Wang and W. Wei, *Energy Storage Materials*, 2020, **32**, 37-45.

12.   E. Zhao, X. Liu, H. Zhao, X. Xiao and Z. Hu, *Chem. Commun.*, 2015, **51**, 9093-9096.

13.   C. Zhang, Y. Feng, B. Wei, C. Liang, L. Zhou, D. G. Ivey, P. Wang and W. Wei, *Nano Energy*, 2020, **75**, 104995.

14.   F. Wu, G. T. Kim, M. Kuenzel, H. Zhang, J. Asenbauer, D. Geiger, U. Kaiser and S. Passerini, *Adv. Energy Mater.*, 2019, **9**, 1902445.

15.   T. Wang, W. Zeng, J. Zhu, W. Tian, J. Wang, J. Tian, D. Yuan, S. Zhang and S. Mu, *Nano Energy*, 2023, **113**,108577.

16.   F. Cao, W. Zeng, J. Zhu, J. Xiao, Z. Li, M. Li, R. Qin, T. Wang, J. Chen and X. Yi, *Small*, 2022, **18**, 2200713.

17.   C. Shen, Y. Liu, L. Hu, W. Li, X. Liu, Y. Shi, Y. Jiang, B. Zhao and J. Zhang, *Nano Energy*, 2022, **101**, 107555.

18.   S. Yang, P. Wang, H. Wei, L. Tang, X. Zhang, Z. He, Y. Li, H. Tong and J. Zheng, *Nano Energy*, 2019, **63**, 103889.